Planar rotation of electric field induced by edge-plasmon in a graphene nanoribbon

M. Shoufie Ukhtary ⓞ,* Masato Maruoka ⓞ, and Riichiro Saito ⓞ
Department of Physics, Tohoku University, Sendai 980-8578, Japan

The presence of an edge in a two-dimensional (2D) material can induce an accumulation of charges near the edge by the electric field. Similar to the 2D plasmon, the accumulated charges can oscillate collectively, forming a distinct plasmon mode, which is called edge-plasmon. In contrast to the 2D plasmon, the electric potential of the edge-plasmon is localized near the edge. In this work, we discuss the edge-plasmon in a 2D material with finite width, such as a graphene nanoribbon, and we find that the localization of the electric field to the edge induces a phase difference of $\pi/2$ between electric fields in the directions parallel and perpendicular to the edge. As a result, the induced electric field rotates on the surface and also induces rotating current, which does not exist in the 2D plasmon. The edge-plasmon can be excited by incident light, and we predict that the rotating current generates rotation of the electric field of the scattered light.

I. INTRODUCTION

A surface plasmon is a collective oscillation of charge density that propagates as an electromagnetic (EM) wave on a surface [1–5]. The surface plasmon has been an interesting platform to confine and control light on a subwavelength scale since the EM fields of the surface plasmon are spatially localized near the surface [1–4]. In particular, we can control the surface plasmon in a two-dimensional (2D) material such as graphene since the charge density of graphene or the Fermi energy E_F can be controlled by using gate voltage [3–9]. As long as we consider the 2D material to be an infinite surface, all the charges of the 2D material oscillate collectively, which forms an intrinsic 2D plasmon with $\sqrt{q}$ dependent on frequency, where q is the wave vector [1,3,4,10]. However, if we consider the region in the vicinity of the edge, there will be an accumulation of charges near the edge. This accumulation of charges can also oscillate collectively when the resonant condition is satisfied and forms the so-called edge-plasmon with the EM fields localized near the edge [5,11–18]. The existence of the edge-plasmon on the surface of a 2D material was theoretically predicted by Fetter [13] and also Song and Rudner [11]. They discussed an edge-plasmon near a single edge of an "infinite" 2D material, and they found that the accumulated charges near the edge oscillate collectively, forming an edge-plasmon, which has a frequency smaller than that of a 2D plasmon [11,13,18].

In this paper, we investigate the edge-plasmon in a 2D material with two edges, such as a graphene nanoribbon, analytically. We show that the edge-plasmon in 2D material consists of two distinct modes with symmetrical and antisymmetrical electric potentials between the two edges. We also consider the retardation effect of the edge-plasmon, which is significant in the case of large E_F and small q [19,20]. Otherwise, the group velocity of the edge-plasmon can be larger than the velocity of light. A more interesting point that we find is that the induced electric field on the surface of 2D material rotates in plane as a function of time due to the localization of the EM fields near the edges. The rotation of electric field is found in the case of 2D plasmon, too, although the rotation is out of plane [21–26]. The rotation of the electric field gives rise to the spin angular momentum of light, for which it is established that the spin of the surface plasmon is transverse to the propagation direction, in contrast to the longitudinal spin of circularly polarized light [21–26]. While the spin direction is in plane for a 2D plasmon, we show that the spin of the edge-plasmon is out of plane.

An edge-plasmon has been observed by using scattering-type scanning near-field microscopy in disk and rectangular graphene [27,28]. The edge-plasmon has more spatial confinement compared with the 2D plasmon, which can be used for imaging applications of spectroscopy and also compact plasmonic circuits made of graphene on the subwavelength scale. By applying an external magnetic field or by using a topological insulator phase as the 2D material, a chiral edge-plasmon is predicted, in which the forward-going edge-plasmon has a different velocity than the backward-going one. Thus, we can specify between forward and backward propagations of electronic signals by using the nonreciprocity of the edge-plasmon, which can be implemented in plasmonic logic circuits [5,11–13,17].

Our goal is to show the effect of ribbon geometry on the dispersion and modes of the edge-plasmon with the retardation effect. By solving the electric field of the edge-plasmon on the surface of a 2D material, we will show that the rotation of electric field on the surface also induces a rotating surface-current, which is absent in the case of a 2D plasmon. The rotating surface current generates a rotating electric field in the surrounding media, and the generated field can be understood as the scattered light with elliptical polarization when we excite the edge-plasmon using incident light. Since E_F of a 2D material can be changed by the gate voltage, the rotation of the induced current can be tuned, which makes the tuning

---

*shoufie@flex.phys.tohoku.ac.jp

of the polarization of scattered light possible. Furthermore, we find that the rotation direction of the electric field on the surface depends on the position in the ribbon relative to the edge, in which the direction is clockwise near one edge and counterclockwise near another edge. This implies that the absorption of circularly polarized light or circular dichroism (CD) by the ribbon depends on the position relative to the edge. This spatial dependence of the CD was observed by Narushima and Okamoto [29], who measured the near-field CD signal as a function of position along an S-shaped nanostructure.

This paper is organized as follows. In Sec. II, we discuss our theoretical method to obtain the dispersion and electric potential of the edge-plasmon with retardation. The main results and discussion are given in Sec. III. In Sec. III, we show the dispersion of the edge-plasmon and also the electric field profile on the surface of a ribbon. The generation of the rotating electric field in the surrounding medium will also be discussed. In Sec. IV, our conclusion is given.

II. THEORETICAL METHODS

Let us begin by solving the dispersion relation of the edge-plasmon. Here we consider the two edges of a 2D material and the retardation effect, which is significant in the case of large E_F and small q [19,20]. Hereafter, we refer to the edge-plasmon in the ribbon geometry (or a 2D material with two edges) as simply the edge-plasmon. In short, the dispersion relation of the edge-plasmon can be obtained by solving the electric potential of the edge-plasmon and applying it to boundary conditions [11,13,17]. To obtain the dispersion of the edge-plasmon with the retardation effect, we use the Lorenz gauge to solve the electric potential on the surface of a 2D material Φ, which is expressed as follows:

$$\left(\nabla^2 - \frac{1}{c^2}\partial_t^2\right)\Phi(x, y, z, t) = \frac{e}{\varepsilon_0}n(x, y, t)\delta(z)\Theta(x)\Theta(w - x),$$

(1)

where $n(x, y, t)\delta(z)$ is the charge density on the surface of a 2D material and the product of the Heaviside function $\Theta(x)\Theta(w - x)$ represents the shape of the 2D material ribbon, where w is the width of the ribbon, as shown in Fig. 1. In the direction of y, we consider a ribbon that is infinitely long. The second term on the left-hand side of Eq. (1) gives the retardation effect, which means that the interaction between charges is not instantaneous. Without the second term, we would obtain the Poisson equation, where the retardation is
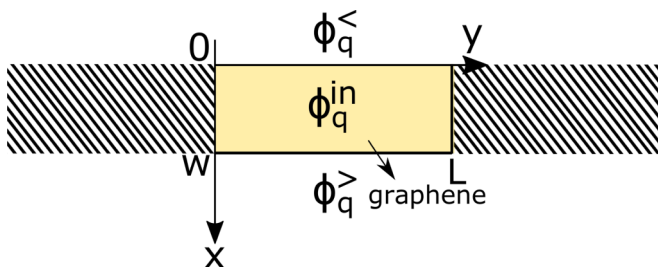

FIG. 1. The 2D material with two edges at $x = 0$ and w seen from above, showing three distinct regions of Eqs. (13)–(15).

neglected [11,13,17]. By assuming plane wave solutions for $\Phi(x, y, t) = \phi_q(x)e^{iqy-i\omega t}$ and $n(x, y, t) = n_q(x)e^{iqy-i\omega t}$ on the surface of a 2D material, where we assume that the edge-plasmon propagates along the y direction, we obtain

$$\left(\partial_x^2 + \partial_z^2 - \kappa^2\right)\phi_q(x, z) = \frac{e}{\varepsilon_0}n_q(x)\delta(z)\Theta(x)\Theta(w - x),$$

(2)

where $\kappa(q, \omega) = \sqrt{q^2 - \omega^2/c^2}$ represents the retarded wave vector. By Fourier transforming Eq. (2) with respect to x,

$$\tilde{\phi}_q(k, z) = \int_{-\infty}^{\infty}dx e^{-ikx}\phi_q(x, z),$$

(3)

$$\tilde{n}_q(k) = \int_{-\infty}^{\infty}dx e^{-ikx}n_q(x)\Theta(x)\Theta(w - x),$$

(4)

we get

$$\left\{\frac{d^2}{dz^2} - (k^2 + \kappa^2)\right\}\tilde{\phi}_q(k, z) = \frac{e}{\varepsilon_0}\tilde{n}_q(k)\delta(z).$$

(5)

The solution of Eq. (5) is given by

$$\tilde{\phi}_q(k, z) = -\frac{e}{2\varepsilon_0}\frac{\tilde{n}_q(k)}{\sqrt{k^2 + \kappa^2}}e^{-\sqrt{k^2+\kappa^2}|z|}.$$

(6)

Hence, the solution of Eq. (5) on the surface ($z = 0$) is expressed as follows:

$$\tilde{\phi}_q(k) = -\frac{e}{2\varepsilon_0}\frac{\tilde{n}_q(k)}{\sqrt{k^2 + \kappa^2}}.$$

(7)

By inverse Fourier transforming Eq. (7) and substituting Eq. (4), we obtain a nonlocal equation to determine the electric potential on the surface as follows:

$$\begin{aligned}\phi_q(x) &= \frac{1}{2\pi}\int_{-\infty}^{\infty}dk e^{ikx}\tilde{\phi}_q(k)\\&= -\frac{e}{4\pi\varepsilon_0}\int_{-\infty}^{\infty}dk\frac{e^{ik(x-x')}}{\sqrt{k^2 + \kappa^2}}\\&\quad\times\int_{-\infty}^{\infty}dx' n_q(x')\Theta(x')\Theta(w-x')\\&= \int_{-\infty}^{\infty}dx' W_q(x - x')n_q(x')\Theta(x')\Theta(w - x'),\end{aligned}$$

(8)

where

$$W_q(x - x') = -\frac{e}{4\pi\varepsilon_0}\int_{-\infty}^{\infty}dk\frac{e^{ik(x-x')}}{\sqrt{k^2 + \kappa^2}}.$$

(9)

$W_q(x - x')$ is called the Coulomb interaction kernel [11]. Since $1/\sqrt{k^2 + \kappa^2}$ is a fast-decaying function of k, we can approximate it to $2\kappa/(k^2 + 2\kappa^2)$ by expanding it around $k^2 = 0$. Then, the interaction kernel becomes [11,13–15]

$$\begin{aligned}W_q(x - x') &\cong -\frac{e}{4\pi\varepsilon_0}\int_{-\infty}^{\infty}dk e^{ik(x-x')}\frac{2\kappa}{k^2 + 2\kappa^2}\\&= -\frac{e}{2\sqrt{2}\varepsilon_0}e^{-\sqrt{2}\kappa|x-x'|}.\end{aligned}$$

(10)

By substituting the approximated $W_q(x - x')$ in Eq. (8), the electric potential $\phi_q(x)$ satisfies the following differential equation:

$$\left(\partial_x^2 - 2\kappa^2\right)\phi_q(x) = \frac{e\kappa}{\varepsilon_0}n_q(x)\Theta(x)\Theta(w - x),$$

(11)

where the charge density $n_q(x)$ is expressed as

$$n_q(x) = \frac{i\sigma(\omega)}{e\omega}\left(-\partial_x^2 + \kappa^2\right)\phi_q(x), \quad (12)$$

which can be obtained from the continuity equation, $-e\partial_t n(x, y, t) + \nabla \cdot \mathbf{J} = 0$ (see details in Appendix A). We adopt $\sigma(\omega) = ie^2 E_F/(\pi\hbar^2\omega)$ as the optical conductivity of a 2D material [1,3,6,11].

By substituting Eq. (12) into Eq. (11), we can solve for $\phi_q(x)$. Due to the step function $\Theta(x)\Theta(w - x)$, we have three distinct solutions of Eq. (11) for three regions (see Fig. 1), given as follows:

$$\phi_q^{in}(x) = \phi_1^+ e^{\gamma_1 x} + \phi_1^- e^{-\gamma_1 x} \quad (0 < x < w), \quad (13)$$

$$\phi_q^<(x) = \phi_0 e^{\gamma_0 x} \quad (x < 0), \quad (14)$$

$$\phi_q^>(x) = \phi_2 e^{-\gamma_0 x} \quad (x > w), \quad (15)$$

where $\gamma_0(q, \omega) = \sqrt{2}\kappa$, γ_1 is given by

$$\gamma_1(q, \omega) = \sqrt{2}\kappa \sqrt{\frac{\frac{2}{\kappa} + \frac{i\sigma(\omega)}{\varepsilon_0\omega}}{\frac{2}{\kappa} + \frac{i2\sigma(\omega)}{\varepsilon_0\omega}}}, \quad (16)$$

and $\phi_1^+, \phi_1^-, \phi_0, \phi_2$ are constants. From Eqs. (13)–(15), we understand that outside the 2D material, the electric potential exponentially decays as we move away from the edges, while inside the 2D material, the electric potential is a linear combination of increasing and decaying functions of the position x due to the presence of the two edges.

To obtain the dispersion of the edge-plasmon, Eqs. (13)–(15) are substituted in the boundary conditions at the positions of edges. The boundary conditions for ϕ_q and $\partial_x\phi_q$ at $x = 0$ are given by

$$\phi_q^<(0) = \phi_q^{in}(0), \quad (17)$$

$$\partial_x\phi_q^<(x)|_{x=0} - \partial_x\phi_q^{in}(x)|_{x=0} = i\frac{\kappa\sigma(\omega)}{\omega\varepsilon_0}\partial_x\phi_q^{in}(x)|_{x=0}. \quad (18)$$

The boundary conditions at $x = w$ are given by

$$\phi_q^{in}(w) = \phi_q^>(w), \quad (19)$$

$$\partial_x\phi_q^{in}(x)|_{x=w} - \partial_x\phi_q^>(x)|_{x=w} = -i\frac{\kappa\sigma(\omega)}{\omega\varepsilon_0}\partial_x\phi_q^{in}(x)|_{x=w}. \quad (20)$$

Equations (17) and (19) come from the fact that the electric potential is continuous at the boundaries. The discontinuity of $\partial_x\phi_q$ in Eqs. (18) and (20) at the edges is due to the charges accumulating at the edges. The derivations of Eqs. (18) and (20) are given in Appendix B. From Eqs. (17) and (18), we obtained the following ratio:

$$\frac{\phi_1^-}{\phi_1^+} = \frac{\gamma_1 - \gamma_0 + D}{\gamma_1 + \gamma_0 + D} \equiv C(q, \omega), \quad (21)$$

where $D(q, \omega) \equiv i\kappa(q, \omega)\sigma(\omega)\gamma_1/(\omega\varepsilon_0)$. Similarly, from Eqs. (19) and (20), we obtained the following ratio:

$$\frac{\phi_1^-}{\phi_1^+} = \frac{\gamma_1 + \gamma_0 + D}{\gamma_1 - \gamma_0 + D}e^{2\gamma_1 w}; \quad (22)$$

Eq. (21) should equal Eq. (22). Therefore, we arrive at the following transcendental equation, from which the dispersion of the edge-plasmon can be solved numerically:

$$(\gamma_1 + \gamma_0 + D) = \pm(\gamma_1 - \gamma_0 + D)e^{-\gamma_1 w}. \quad (23)$$

III. RESULTS AND DISCUSSION

A. Dispersion of an edge-plasmon in a ribbon

In Fig. 2(a), we plot the frequency of the edge-plasmon ω as a function of the wave vector q, which is obtained by solving Eq. (23) for $E_F = 0.64$ eV and $w = 30$ μm. In Fig. 2(a), we show the two lowest-energy solutions of Eq. (23), which correspond to the $\pm$ sign in Eq. (23). The lower- (higher-) energy solution, denoted by ω_+ (ω_-), comes from the $+$ ($-$) sign in Eq. (23). We also compare the analytical dispersions
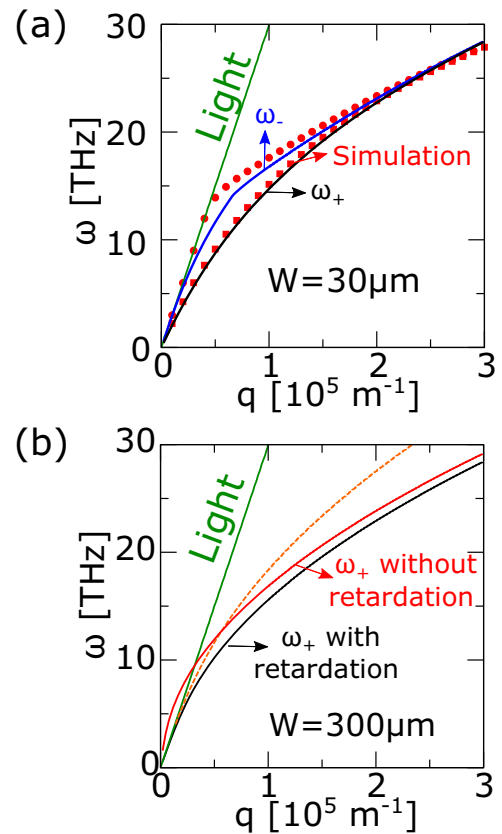

FIG. 2. (a) The dispersions of the edge-plasmon obtained by solving Eq. (23), denoted by ω_+ (black line) and ω_- (blue line), which correspond to the $\pm$ sign in Eq. (23). The FDTD simulation results are denoted by the dots. Here we use $E_F = 0.64$ eV and $w = 30$ μm. (b) ω_+ with and without the retardation effect for a ribbon with $w = 300$ μm. If the retardation effect is excluded, the group velocity of the edge-plasmon can be larger than the velocity of light at small q. With the retardation effect, the dispersion of the edge-plasmon is always below the dispersion of light. The orange dashed line is dispersion of the 2D plasmon.
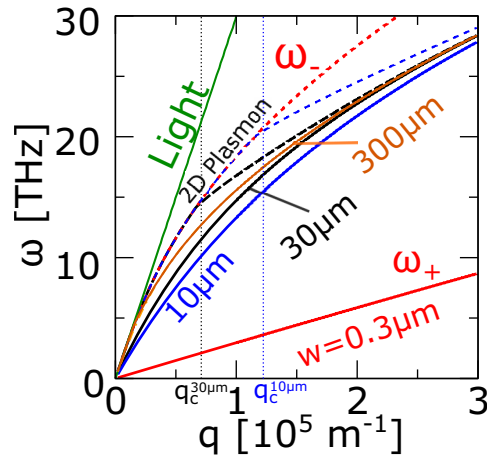
FIG. 3. ω_+ and ω_- for $w = 0.3\ \mu m$ (pink), $10\ \mu m$ (blue), $30\ \mu m$ (black), and $300\ \mu m$ (orange). Here ω_+ is shown as solid lines, while ω_- is shown as dashed lines. For $w = 300\ \mu m$, ω_+ and ω_- overlap, which is nothing but the dispersion of the edge-plasmon with only one edge. Here we adopt $E_F = 0.64$ eV. q_c is the wave vector where the derivative of the ω_- curve is discontinuous.

with the ones obtained from a finite-difference time-domain (FDTD) simulation using the MEEP software [30], which are shown as the red dots in Fig. 2(a). For most wave vectors, our analytical dispersion relations match well with the simulated ones and behave similarly. For example, at $q > 2 \times 10^5$ m^{-1}, the analytical dispersion curves almost overlap each other in Fig. 2(a), which is also shown by the simulated ones. For much larger q ($qw \gg 1$), ω_+ and ω_- are degenerate since $\Delta\omega \equiv \omega_- - \omega_+ \ll 1/\tau$, where τ is the lifetime of the edge-plasmon. Since we do not calculate the lifetime of the edge-plasmon, we approximate τ as the lifetime of a graphene 2D plasmon, which is on the order of 10^{-8} s [31]. Furthermore, ω_+ and ω_- overlap with the frequency of the edge-plasmon if we consider only one edge. This is because at $qw \gg 1$, the wavelength of the edge-plasmon is much shorter than w, which means the presence of another edge is neglected and the edge-plasmon is localized at only one edge.

Here we point out the importance of the retardation effect. In Fig. 2(b), we show only ω_+ with and without the retardation effect as a function of q for $E_F = 0.64$ eV and $w = 300\ \mu m$. In this case, we increase w in order to see the retardation effect more clearly. It is noted that ω_- has almost the same frequency as ω_+ even for $q = 10^4$ m^{-1}. Without the retardation effect, ω_+ intersects the dispersion of light, and for a wave vector smaller than the intersection point or retarded regime, the group velocity of the edge-plasmon is larger than the velocity of light, which is not physical. By including the retardation effect, the frequency of the edge-plasmon is reduced, and the dispersion is always below the dispersion of light. In the retarded regime, the dispersion of the edge-plasmon is linear following the dispersion of light. Similar to the case of a 2D plasmon in graphene, the retarded regime becomes wider with increasing E_F [19,20] and also with increasing w.

In Fig. 3, we show the calculated dispersion of the edge-plasmon with several values of w for $E_F = 0.64$ eV. Here ω_+ is shown by solid lines, while ω_- is shown by dashed

lines. In the case of $w = 0.3\ \mu m$ ($qw \ll 1$), ω_+ and ω_- are much separated. ω_+ disperses linearly to q, while ω_- has $\sqrt{q}$ dependence, which is nothing but the dispersion of a 2D plasmon. ω_- for $qw \ll 1$ can be shown easily from Eq. (23) by assuming $e^{-\gamma_1 w} = 1$. Then, we arrive at the following equation for the ω_- branch:

$$(\gamma_1 + \gamma_0 + D) = (\gamma_0 - \gamma_1 - D). \tag{24}$$

Since $D(q, \omega) \equiv i\kappa(q, \omega)\sigma(\omega)\gamma_1/(\omega\varepsilon_0)$, the solution of Eq. (24) is given by the solution of $\gamma_1 = 0$. $\gamma_1 = 0$ implies that the potential in the ribbon is uniform across the width, as shown by Eq. (13); in other words, we have a 2D plasmon. γ_1 vanishes if the following condition is fulfilled:

$$\frac{2}{\kappa} + \frac{i\sigma(\omega)}{\varepsilon_0\omega} = 0, \tag{25}$$

which is exactly the requirement of a 2D plasmon [1]. Therefore, ω_- is a 2D plasmon when $qw \ll 1$.

The separation between ω_+ and ω_- decreases with increasing w. The discontinuity in the derivative of the dispersion curve of ω_- at q_c as shown in Fig. 3 comes from the change in the 2D plasmon solution ($q < q_c$) to an edge-plasmon solution ($q > q_c$). The edge-plasmon starts to exist at the point of discontinuity where γ_1 has a nonzero real value. For ($q > q_c$), ω_- continues to disperse while approaching ω_+. For $w = 300\ \mu m$ or $qw \gg 1$, ω_+ and ω_- are degenerate and overlap in one dispersion, which is nothing but the dispersion of the edge-plasmon with only one edge.

It is noted that for a very small width of the graphene ribbon, the nonlocality of graphene conductivity $\sigma(q, \omega)$ can affect the dispersion and modes of the edge-plasmon. Wang and Kinaret [32] and Thongrattanasiri *et al.* [33] have shown that the nonlocality effect increases the plasmon frequency for graphene nanostructure with a size less than 10 nm. The nonlocality also decreases the charge density near the edges, which makes the potential and charge density less bound to the edges. In the present results, the smallest width that we use is $0.3\ \mu m = 300$ nm, which is sufficiently large to not discuss nonlocality; therefore, the nonlocality effect can be neglected. The nonlocality effect may appear for a width of 300 nm at large frequency and wave vector. If we include the nonlocality for a width of 300 nm, by using the nonlocal conductivity given by Wang and Kinaret [32], the frequency correction is less than 1% even at $\omega = 120$ THz and at $q = 7 \times 10^6$ m^{-1}, and the correction increases with further increasing q, where it reaches 4% at $\omega = 290$ THz and at $q = 3 \times 10^7$ m^{-1}.

B. Electric potential and field on the surface of the ribbon

In Figs. 4(a) and 4(b), we show the electric potential ϕ_q as a function of position x, which is given by Eqs. (13)–(15), for ω_+ and ω_-, respectively. The constants in Eqs. (13)–(15) are obtained from the boundary conditions, and we set $\phi_1^- = 1$. We show the cases of $q = 10^5$ and 10^6 m^{-1}, which correspond, respectively, to $qw = 3$ and 30 for $w = 30\ \mu m$ or $qw \geqslant 1$. We refer to ϕ_q for the ω_+ branch as the symmetrical mode due to the symmetry of ϕ_q between the two edges, while we refer to the ω_- branch as the antisymmetrical mode. In all cases, ϕ_q has a maximum value in the edges of ribbon, and the localization of ϕ_q near both edges is more pronounced when q
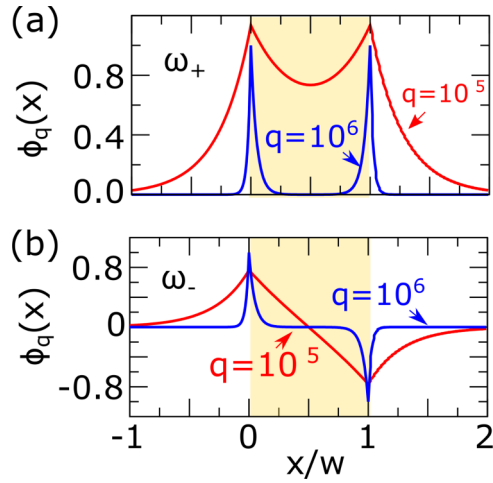
FIG. 4. (a) and (b) The electric potentials ϕ_q as a function of position x for ω_+ and ω_-, respectively. Graphene width is shown as the shaded area. Here we adopt $E_F = 0.64$ eV and $w = 30\ \mu$m. $q = 10^5$ and 10^6 m^{-1} correspond, respectively, to $qw = 3$ and 30 for $w = 30\ \mu$m.

is increased ($qw \gg 1$) since $1/\gamma_1 \ll w$, which means that the edge-plasmon at one edge cannot recognize another edge.

Let us discuss ϕ_q for $qw \ll 1$. In Fig. 5, we show only ϕ_q with $q = 10^4$ m^{-1} as a function of position x for the symmetrical (ω_+) mode since the antisymmetrical (ω_-) mode does not exist. For the ω_+ mode, ϕ_q is almost uniform across the width since $1/\gamma_1 \gg w$. ϕ_q of the edge-plasmon at each edge decays as a function of x, but since ϕ_q inside the ribbon is a combination of ϕ_q of both edge-plasmons at two edges, then the decaying ϕ_q is not pronounced, and ϕ_q looks uniform.

In Fig. 6, we show the charge density $n(x, y, t = 0)$ of the edge-plasmon as a function of position x and y for several q. n is calculated from Eq. (12). Similar to ϕ_q, n is localized near the edges of the ribbon, and the localization of n is more pronounced when $qw \gg 1$. The case of $q = 10^5$ m^{-1} is given by Figs. 6(a) and 6(b) for the ω_+ and ω_- modes, respectively, while the case of $q = 10^6$ m^{-1} is given by Figs. 6(c) and 6(d) for the ω_+ and ω_- modes, respectively. As we can see in Fig. 6, for the ω_+ mode, the propagation of the charge density n in both edges is in phase as a function of y, while in the ω_- mode, the propagation is out of phase. It is noted that for
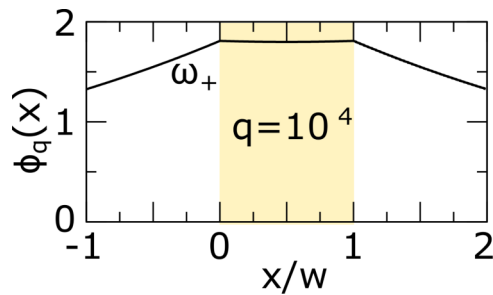

FIG. 5. The electric potentials ϕ_q as a function of position x for the symmetrical (ω_+) mode with $q = 10^4$ m^{-1}, which corresponds to $qw = 0.3$. Only the symmetrical mode exists. Here we adopt $E_F = 0.64$ eV and $w = 30\ \mu$m.
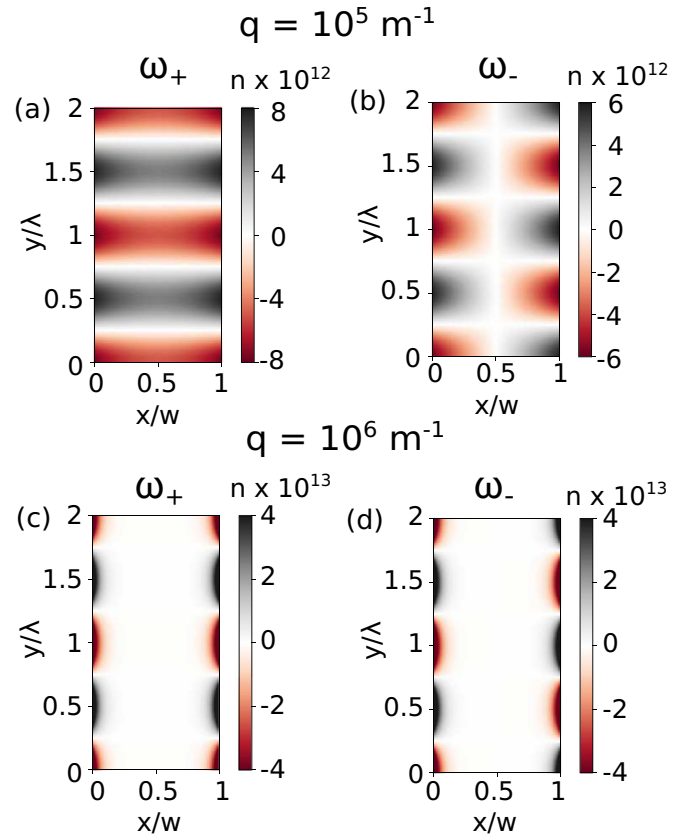

FIG. 6. The charge density $n(x, y, t = 0)$ (in $1/$m^2) as a function of positions x and y. Black, red, and white denote the positive, negative, and zero charge densities. The left and right columns correspond to ω_+ and ω_- edge-plasmons, respectively. The wave vectors $q = 10^5$ and 10^6 m^{-1} are given for (a) and (b), and (c) and (d), respectively. Here we adopt $E_F = 0.64$ eV and $w = 30\ \mu$m.

the case of $qw \ll 1$ (not shown), where we have only the ω_+ mode, n is almost uniform across the width due to the long decay length.

The localization of the electric potential near the edges gives an interesting phenomenon which does not exist in the case of the 2D plasmon. In the case of an edge-plasmon, the electric field on the surface rotates in plane as a function of time; in other words, E_x and E_y have a $\pi/2$ phase difference. The rotation of the electric field can also be found in the case of the 2D plasmon, but the rotation is out of plane [21–26]. Therefore, the induced surface current will also rotate in the case of the edge-plasmon, which is not found in the 2D plasmon. The electric field of the edge-plasmon on the surface of graphene can be obtained from $E_r(x, y, t) = -\partial_r \Phi(x, y, t)$, where $\Phi(x, y, t) = \phi_q(x) e^{iqy - i\omega t}$ and $r = x, y$. The electric fields are given as follows:

$$E_x(x, y, t) = -\gamma_1(\phi_1^+ e^{\gamma_1 x} - \phi_1^- e^{-\gamma_1 x}) e^{iqy - i\omega t},$$

$$E_y(x, y, t) = -iq(\phi_1^+ e^{\gamma_1 x} + \phi_1^- e^{-\gamma_1 x}) e^{iqy - i\omega t}. \quad (26)$$

In Fig. 7, we plot the electric fields as a function of time for $q = 10^5$ m^{-1} at the position of both edges ($x = 0$ and $x = w$). Figures 7(a) and 7(b) show the electric fields for the symmetrical mode, while Figs. 7(c) and 7(d) show the
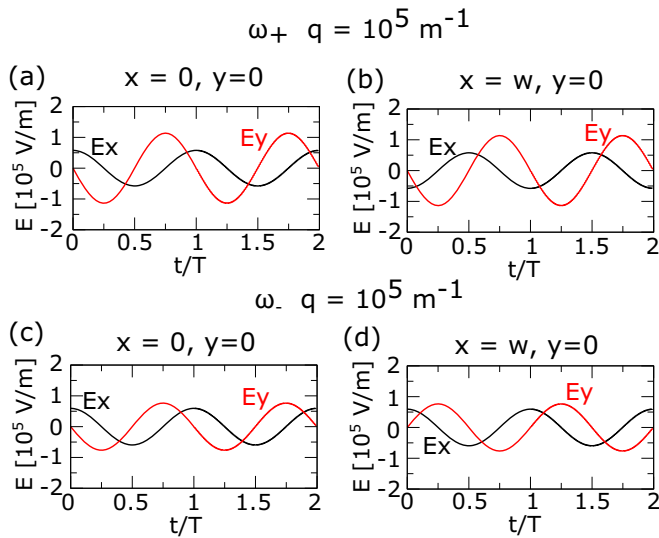
FIG. 7. The electric fields (E_x and E_y) as a function of time for $q = 10^5$ m^{-1} at the position of both edges ($x = 0$ and $x = w$). $T = 2\pi/\omega$ is the period of the edge-plasmon. (a) and (b) show the electric fields for the symmetrical mode, while (c) and (d) show the antisymmetrical mode. Here we use $E_F = 0.64$ eV and $w = 30$ μm.

FIG. 8. (a) The electric field profiles for symmetrical and anti-symmetrical modes as the time increases (from top to bottom). The size of the arrow corresponds to the magnitude of the electric field. Near edge $x = 0$, the rotation of the electric field is clockwise, while at another edge, $x = w$, the rotation is counterclockwise. (b) Due to the planar rotation of the electric field, the edge-plasmon has out-of-plane optical spin S, which has opposite directions near both edges. Here $q = 10^5$ m^{-1}, $E_F = 0.64$ eV, and $w = 30$ μm.

antisymmetrical mode. In all cases, there is a $\pi/2$ phase difference between E_x and E_y, which means that the electric field rotates on the surface. The cross section of the rotation for the antisymmetrical mode is almost circular since the amplitudes of E_x and E_y are almost the same, while for the symmetrical mode, the cross section is more elliptic. Furthermore, the rotation directions at both edges are opposite each other. In fact, at $x = 0$, the rotation is clockwise, while at $x = w$ the rotation is counterclockwise.

To understand the rotation of the electric field on the surface, in Fig. 8(a), we plot the electric field as a function of position x and y at several increasing t ($t < T$) for both symmetrical and antisymmetrical modes for $q = 10^5$ m^{-1}. The magnitude of the electric field decays as we move from the edges; thus, it is minimum at the center of the width. The rotation directions at both edges are opposite each other since the decay directions in the ribbon at both edges are also opposite. For the edge at $x = 0$, the field decays in the positive x direction, while for the edge at $x = w$, the field decays in the negative x direction. The origin of the rotation is the fact that wave vectors in the direction of the ribbon length are a real value, while the one in the direction perpendicular to the ribbon length is an imaginary value. This gives a $\pi/2$ phase difference between E_y and E_x as a function of time. The rotation of the electric field gives rise to the spin angular momentum of light, which is referred to as optical spin, whose direction is perpendicular to the cross section of rotation [21–26]. Since the electric field of the edge-plasmon rotates on the surface of graphene, the edge-plasmon has optical spin perpendicular to the ribbon plane or out-of-plane spin and also transverse to the direction of propagation q, as illustrated in Fig. 8(b). This out-of-plane spin sets the edge-plasmon apart from the 2D plasmon because the spin of the 2D plasmon is in plane, as mentioned before. Another interesting finding is that the directions of optical spins of the edge-plasmon at
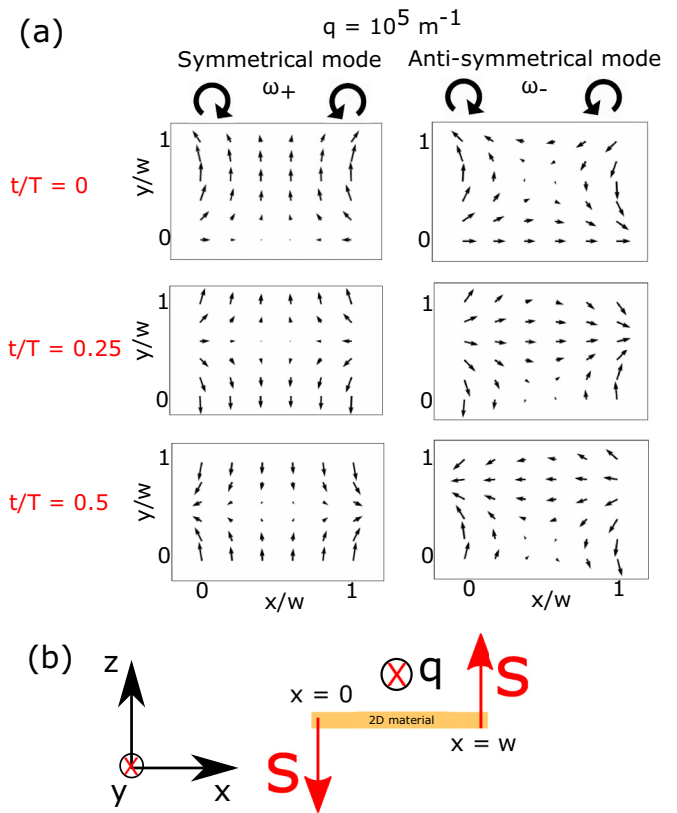
both edges are opposite each other, even though the edge-plasmon propagates in one direction. In other words, the light propagates on the surface with spatially separated spin, as illustrated in Fig. 8(b).

Let us discuss the effect of loss on the $\pi/2$ phase difference. The loss is defined as the imaginary part of the frequency, which is denoted by Γ, $\hbar\omega \to \hbar\omega + i\Gamma$. When we include the loss, γ_1 in Eq. (16) has an imaginary part. Then, the direction of the main axis of the ellipsoidal electric field on the plane is tilted (about $1°$ for $\Gamma = 11$ meV) because $E_x/E_y \cong \gamma_1/iq$ has a real part. In other words, the phase difference is not exactly $\pi/2$ due to the loss but is very close to $\pi/2$ (about $1°$ smaller).

In Fig. 9, we show the ellipticity $|E_x|/|E_y|$ of the electric field at the surface as a function of loss Γ for $q = 1 \times 10^5$ m^{-1} and the ω_+ mode. Since the change in phase difference is only $1°$ for $\Gamma = 11$ meV, the ellipticity can still be defined as $|E_x|/|E_y|$. In Fig. 9, diamonds and circles denote, respectively, the ellipticity for field at $x = 0$ and w. For small loss ($\Gamma < 1$ meV), the ellipticities at both edges are the same, but as we increase the loss, the ellipticity at $x = 0$ decreases monotonically, while the one at $x = w$ increases. Eventually,
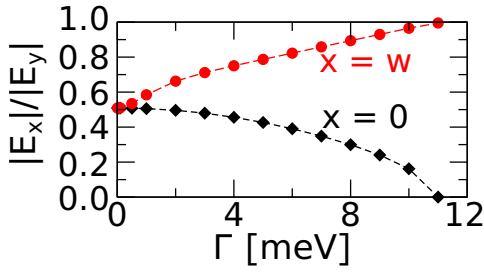
FIG. 9. The ellipticity $|E_x|/|E_y|$ of the electric field at the surface as a function of loss Γ for $q = 1 \times 10^5$ m^{-1} and the ω_+ mode.

the ellipticity at $x = 0$ vanishes at large Γ, while it reaches 1 for $x = w$.

Let us discuss the surface current induced by the edge-plasmon. The surface current in the direction of $r = x, y$ can be obtained from Ohm's law $J_r = \sigma(\omega)E_r$. Thus, the surface current is given by

$$J_x(x, y, t) = -\sigma(\omega)\gamma_1(\phi_1^+ e^{\gamma_1 x} - \phi_1^- e^{-\gamma_1 x})e^{iqy-i\omega t},$$
$$J_y(x, y, t) = -i\sigma(\omega)q(\phi_1^+ e^{\gamma_1 x} + \phi_1^- e^{-\gamma_1 x})e^{iqy-i\omega t}, \quad (27)$$

where it is obvious that J_x and J_y have a $\pi/2$ phase difference from the factor of i in J_y similar to the electric field. Thus, in the case of the edge-plasmon, the vector of the surface current **J** rotates as a function of time, which is not found in the case of a 2D plasmon. The rotating surface-current induces a rotating electric field in the surrounding medium, which has a plane of rotation parallel to the surface of the 2D material. This implies that when we excite the edge-plasmon using linearly polarized light, the scattered light will be elliptically polarized light, which is illustrated in Fig. 10(a). In the case where the edge-plasmon is not excited, such as in the case of an ordinary light-scattering process or excitation of a 2D plasmon, the induced current does not have rotation; therefore, the scattered light is linearly polarized, as illustrated in Fig. 10(b).

It is noted that the rotation direction of the surface current depends on the position relative to the edges. This means that the absorption of the circularly polarized light of the ribbon depends on the position. From Fig. 8, we can say that the left-handed polarized light is absorbed near $x = 0$ and the right-handed light is absorbed near $x = w$. This spatial dependence
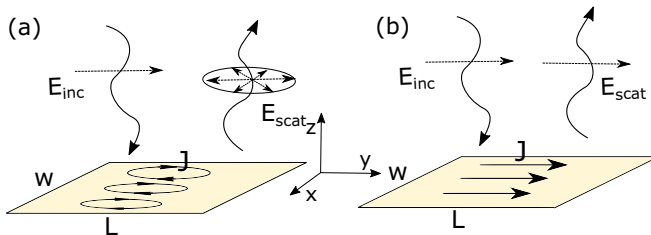

FIG. 10. (a) When the edge-plasmon is excited, the induced current J has two components, whose phase difference is $\pi/2$. Therefore, J is rotating on the surface as a function of time, which generates scattered light with the rotating electric field. (b) On the other hand, in an ordinary light-scattering process, J is not rotating, which generates scattered light with linear polarization. The 2D material has a width of w and length of L.

of absorption of circularly polarized light due to the presence of two edges might be related to the spatial dependence of the circular dichroism observed by Narushima and Okamoto, who measured the near-field CD signal as a function of the position along an S-shaped nanostructure [29].

C. Generation of the electric field from the surface current

The scattered light can be considered the radiation from the induced surface current **J** [34,35]. The generated electric field of the scattered light **E**^{s} can be calculated from [36]

$$\mathbf{E^s}(x, y, z, t) = i\omega\mu_0 \int_0^L dy' \int_0^w dx' \bar{\bar{\mathbf{G}}}(x', y', z)\mathbf{J}(x', y', t), \quad (28)$$

where the Green's function tensor $\bar{\bar{\mathbf{G}}}(x', y', z)$ can be calculated by [36]

$$\bar{\bar{\mathbf{G}}}(x', y', z)) = \left[\bar{\bar{\mathbf{I}}} + \frac{1}{k^2}\nabla\nabla\right]\frac{e^{ikR}}{4\pi R}, \quad (29)$$

where $k = \omega/c$ is the wave vector of scattered light, $R = \sqrt{(x - x')^2 + (y - y')^2 + z^2}$, and $\bar{\bar{\mathbf{I}}}$ is a unit tensor. In the calculation of Eq. (28), we take the finite length of the ribbon L, and the current is given by Eq. (27). This treatment can be found in the treatment of the traveling-wave antenna [35].

From Fig. 8(a), for $q = 10^5$ m^{-1}, we understand that the rotation directions at both edges are opposite each other; therefore, the scattered light at the far field is linearly polarized. However, when we increase q ($qw \gg 1$), the ω_+ and ω_- modes are degenerate. Thus, the corresponding excited mode is the linear combination of symmetrical and antisymmetrical modes, which are shown in Figs. 4(a) and 4(b), respectively. As a result, the electric potential of the excited mode is localized near one edge ($x = 0$), which is shown in Fig. 11(a), and the surface current rotates in one direction (clockwise), which generates a rotating electric field in the surrounding medium.

In Figs. 11(b) and 11(c), we show **E**^{s} as a function of time for $q = 10^6$ m^{-1}, which is calculated from Eq. (28) at $z = 10^3 w$, $x = 0.5w$, $y = 2.5w$ and $z = 10^3 w$, $x = 0.5w$, $y = 10^3 w$, respectively, which correspond to the far field. In both cases, E_x^s and E_y^s have different phases of $\pi/2$, which gives rise to rotating **E**^{s} as a function of time. The rotation of **E**^{s} originates from the rotation of **J**. It is noted that for Fig. 11(c), E_z^s appears, which means that the rotation cross-section is not in the xy plane but tilted to the z axis. It is found that in all the degenerate cases ($qw \gg 1$), the ellipticity of the generated electric field can be approximated by γ_1/q, which is almost constant as a function of q and E_F. In fact, the value of γ_1/q for $q = 10^6$ m^{-1} is 0.7.

The edge-plasmon can be excited optically by using a prism or grating to match the wave vector of the incident light and edge-plasmon. Similar to the case of a 2D plasmon excitation, p-polarized incident light is needed to excite the edge-plasmon; the difference is only the resonant frequency. It is noted that in Fig. 11(a), the total electric potential is localized near left edge since we set $\phi_1^- = 1$ and $\phi_1^+ = \phi_1^-/C(q, \omega)$. The localization position depends on the values of ϕ_1^- and ϕ_1^+. If we set $\phi_1^+ = 1$ and $\phi_1^- = \phi_1^+ \times C(q, \omega)$, the
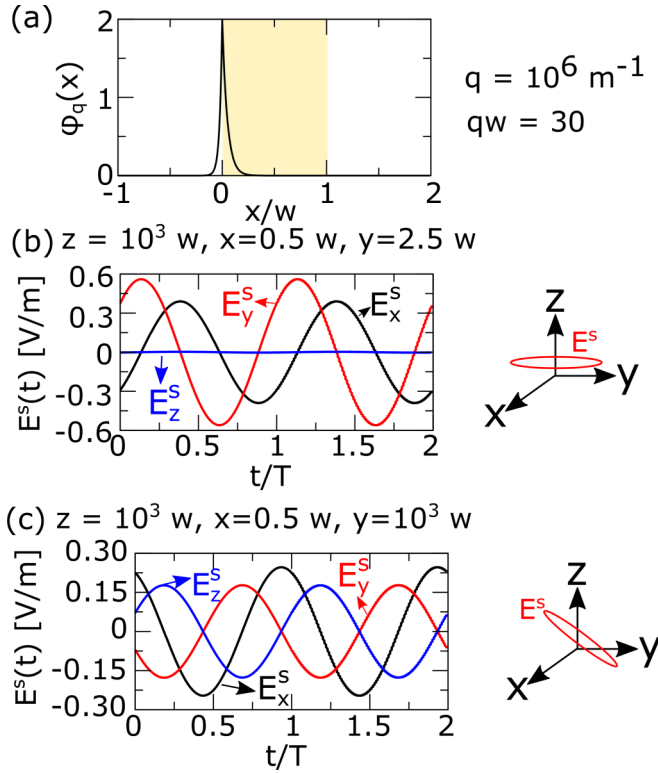
FIG. 11. (a) The electric potential of the excited mode for $q = 10^6$ m^{-1} ($qw \gg 1$), where the modes are degenerate. The generated electric fields as a function of time at the position (b) $z = 10^3 w$, $x = 0.5w$, $y = 2.5w$ and (c) $z = 10^3 w$, $x = 0.5w$, $y = 10^3 w$. The rotation cross-sections of $\mathbf{E}^s$ for both cases are given. Here we adopt $E_F = 0.64$ eV, $w = 30$ μm and $L = 5w$.

localization position is at the right edge. Thus, we can have localization at the left or right edge depending on the values of ϕ_1^- and ϕ_1^+, which are determined by the intensity and position of the incident light relative to the edges.

Since q is related to the incident angle, then by fixing the frequency of the incident light ω and E_F, q is determined from the dispersion relation, and the incident angle is determined accordingly. By selecting ω with $qw \gg 1$, the scattered light will be rotating, as shown by Fig. 11. Then, if E_F is changed while keeping ω and the incident angle, the resonant condition is not satisfied anymore, which means the scattered light has linear polarization since the surface current is not rotating. Therefore, we can tune the polarization of scattered light to be linear or elliptic by changing E_F.

IV. CONCLUSION

In this work, we studied the edge-plasmon, which is a plasmon that is localized near the edge of a 2D material. We showed that the presence of two edges in the 2D material creates two distinct modes of the edge-plasmon due to the interaction between the edge-plasmons of both edges. However, for $qw \gg 1$, the two modes of the edge-plasmon are degenerate, and the edge-plasmon is localized near one of the edges. We also included the retardation effect in our calculation, so that the group velocity of the edge-plasmon never exceeds the velocity of light.

The more interesting finding is that we showed the planar rotation of the electric field of the edge-plasmon. The electric field rotates clockwise near one edge and counterclockwise near another edge as a function of time. The planar rotation of the electric field is interpreted as the out-of-plane spin of light, in contrast to the in-plane spin of light in the case of the 2D plasmon. The directions of spin near both edges are opposite each other. The planar rotation of the electric field also induces a rotating surface-current, which generates a rotating electric field in the surrounding medium. This implies that when we excite the edge-plasmon using linearly polarized light, the scattered light will be elliptically polarized. Due to the dependence of frequency of the edge-plasmon on E_F, the tuning of the polarization of scattered light by E_F is possible. Thus, the planar rotation of the electric field can be observed experimentally by observing the elliptically polarized light generated from the graphene ribbon. Another way to observe the rotation of the electric field is by observing the spin of a metallic nanoparticle placed on the surface of the ribbon, where we expect that the nanoparticle spins in the out-of-plane direction due to the optical torque exerted by the edge-plasmon [21,25].

APPENDIX A: THE CHARGE DENSITY

The charge density $n_q(x)$ in Eq. (12) can be obtained from the continuity equation as follows:

$$-e\partial_t n(x, y, t) + \nabla \cdot \mathbf{J}(x, y, t) = 0, \tag{A1}$$

where the current $\mathbf{J}$ is given by $\mathbf{J}(x, y, t) = \sigma \mathbf{E}(x, y, t)\Theta(x)\Theta(w - x)$. We assume the plane wave solution of $n(x, y, t)$ and $\Phi(x, y, t)$; then we obtain

$$i\omega e n_q(x)e^{iqy - i\omega t} + \sigma(\omega)\Theta(x)\Theta(w - x)\nabla \cdot \mathbf{E}(x, y, t)$$
$$+ \sigma(\omega)E_x(x, y, t)[\Theta(w - x)\delta(x) - \Theta(x)\delta(w - x)] = 0. \tag{A2}$$

The second term in Eq. (A2) gives the charge density of the ribbon (bulk charge density), which is Eq. (12), while the third and fourth terms give the accumulated charge in edges $x = 0$ and $x = w$, respectively, which are used in the boundary conditions of Eqs. (18) and (20). Let us derive the bulk charge density of Eq. (12); then we focus on the first and second terms of Eq. (A2) as follows:

$$n_q(x) = \frac{i\sigma(\omega)e^{-iqy + i\omega t}}{e\omega}\nabla \cdot \mathbf{E}(x, y, t) \tag{A3}$$

$$= \frac{i\sigma(\omega)e^{-iqy + i\omega t}}{e\omega}\{-\nabla^2\phi_q(x)e^{iqy - i\omega t} - \partial_t\nabla \cdot \mathbf{A}(x, y, t)\} \tag{A4}$$

$$= \frac{i\sigma(\omega)}{e\omega}\left\{-\partial_x^2\phi_q(x) + q^2\phi_q(x) - \frac{\omega^2}{c^2}\phi_q(x)\right\} \tag{A5}$$

$$= \frac{i\sigma(\omega)}{e\omega}(-\partial_x^2 + \kappa^2)\phi_q(x), \tag{A6}$$

where we use the Lorenz gauge $\nabla \cdot \mathbf{A}(x, y, t) = -1/c^2 \partial_t \Phi(x, y, t)$ and $\kappa^2 = q^2 - \omega^2/c^2$. Equation (A6) is nothing but Eq. (12) in the main text.

APPENDIX B: THE BOUNDARY CONDITIONS

At the edges, the electric potential should satisfy the boundary conditions given by Eqs. (17)–(20). In this Appendix, we focus on the detail of the boundary condition involving the discontinuity of the derivative of the electric potential due to the accumulated charge. Let us take the edge at $x = 0$. The accumulated charge density n_q^e is given by the third term in Eq. (A2) as follows:

$$n_q^e(x) = -\frac{\sigma(\omega)}{ie\omega} E_x(x, y, t) \delta(x) e^{-iqy + i\omega t}. \quad \text{(B1)}$$

Then, the discontinuity of the derivative of the electric potential due to n_q^e is given by

$$\partial_x \phi_q^<(x)\big|_{x=0} - \partial_x \phi_q^{\text{in}}(x)\big|_{x=0} \quad \text{(B2)}$$

$$= \int_{-\infty}^{\infty} dx' \left\{ \partial_x W_q(x - x')\big|_{x=0-} - \partial_x W_q(x - x')\big|_{x=0+} \right\}$$
$$\times n_q^e(x') \Theta(x') \Theta(w - x') \quad \text{(B3)}$$

$$= \{\partial_x W_q(x)\big|_{x=0-} - \partial_x W_q(x)\big|_{x=0+}\} \frac{\sigma(\omega)}{ie\omega} \partial_x \phi_q^{\text{in}}(x)\big|_{x=0}. \quad \text{(B4)}$$

The derivative of $W_q(x)$ is obtained from Eq. (10) as follows:

$$\partial_x W_q(x) = \frac{e\kappa}{2\varepsilon_0} \frac{x}{|x|} e^{-\sqrt{2}\kappa|x|}. \quad \text{(B5)}$$

Then, Eq. (B4) becomes

$$\partial_x \phi_q^<(x)\big|_{x=0} - \partial_x \phi_q^{\text{in}}(x)\big|_{x=0} = \frac{i\kappa\sigma(\omega)}{\omega\varepsilon_0} \partial_x \phi_q^{\text{in}}(x)\big|_{x=0}. \quad \text{(B6)}$$

Equation (B6) is nothing but Eq. (18) in the main text. For another edge at $x = w$, we can use a similar method to obtain Eq. (20) in the main text.

[1] M. Jablan, H. Buljan, and M. Soljačić, Plasmonics in graphene at infrared frequencies, Phys. Rev. B **80**, 245435 (2009).

[2] S. A. Maier, *Plasmonics: Fundamentals and Applications* (Springer, Bath, 2007).

[3] S. A. Mikhailov and K. Ziegler, New Electromagnetic Mode in Graphene, Phys. Rev. Lett. **99**, 016803 (2007).

[4] Y. V. Bludov, A. Ferreira, N. M. R. Peres, and M. I. Vasilevskiy, A primer on surface plasmon-polaritons in graphene, Int. J. Mod. Phys. B **27**, 1341001 (2013).

[5] D. R. Mason, S. G. Menabde, S. Yu, and N. Park, Plasmonic excitations of 1D metal-dielectric interfaces in 2D systems: 1D surface plasmon polaritons, Sci. Rep. **4**, 4536 (2014).

[6] F. H. L. Koppens, D. E. Chang, and F. J. Garcia de Abajo, Graphene plasmonics: A platform for strong light–matter interactions, Nano Lett. **11**, 3370 (2011).

[7] R. Saito, K. Sato, P. T. Araujo, D. L. Mafra, and M. S. Dresselhaus, Gate modulated Raman spectroscopy of graphene and carbon nanotubes, Solid State Commun. **175**, 18 (2013).

[8] M. S. Ukhtary, E. H. Hasdeo, A. R. T. Nugraha, and R. Saito, Fermi energy-dependence of electromagnetic wave absorption in graphene, Appl. Phys. Express **8**, 055102 (2015).

[9] W. Gao, G. Shi, Z. Jin, J. Shu, Q. Zhang, R. Vajtai, P. M. Ajayan, J. Kono, and Q. Xu, Excitation and Active Control of Propagating Surface Plasmon Polaritons in Graphene, Nano Lett. **13**, 3698 (2013).

[10] E. H. Hwang and S. Das Sarma, Dielectric function, screening, and plasmons in two-dimensional graphene, Phys. Rev. B **75**, 205418 (2007).

[11] J. C. W. Song and M. S. Rudner, Chiral plasmons without magnetic field, Proc. Natl. Acad. Sci. USA **113**, 4658 (2016).

[12] A. Kumar, A. Nemilentsau, K. H. Fung, G. Hanson, N. X. Fang, and T. Low, Chiral plasmon in gapped Dirac systems, Phys. Rev. B **93**, 041413(R) (2016).

[13] A. L. Fetter, Edge magnetoplasmons in a bounded two-dimensional electron fluid, Phys. Rev. B **32**, 7676 (1985).

[14] W. Wang, J. M. Kinaret, and S. P. Apell, Excitation of edge magnetoplasmons in semi-infinite graphene sheets: Temperature effects, Phys. Rev. B **85**, 235444 (2012).

[15] J. W. Wu, P. Hawrylak, G. Eliasson, and J. J. Quinn, Theory of the Lateral Surface Magnetoplasmon in a Semiconductor Superlattice, Phys. Rev. B **33**, 7091 (1986).

[16] A. Y. Nikitin, F. Guinea, F. J. Garcia-Vidal, and L. Martin-Moreno, Edge and waveguide terahertz surface plasmon modes in graphene microribbons, Phys. Rev. B **84**, 161407(R) (2011).

[17] Y. Zhang, J. Gu, and F. Zhai, Edge modes of chiral Berry plasmons in graphene nanoribbons, Phys. Rev. B **99**, 195450 (2019).

[18] W. Wang, P. Apell, and J. Kinaret, Edge plasmons in graphene nanostructures, Phys. Rev. B **84**, 085423 (2011).

[19] H. Y. Deng and K. Wakabayashi, Retardation effects on plasma waves in graphene, topological insulators, and quantum wires, Phys. Rev. B **92**, 045434 (2015).

[20] M. S. Ukhtary and R. Saito, Quantum description of surface plasmon excitation by light in graphene, Phys. Status Solidi B **255**, 1800181 (2018).

[21] K. Y. Bliokh and F. Nori, Transverse and longitudinal angular momenta of light, Phys. Rep. **592**, 1 (2015).

[22] K. Y. Bliokh and F. Nori, Transverse spin of a surface polariton, Phys. Rev. A **85**, 061801(R) (2012).

[23] K. Y. Bliokh, J. Dressel, and F. Nori, Conservation of the spin and orbital angular momenta in electromagnetism, New J. Phys. **16**, 093037 (2014).

[24] F. Kalhor, T. Thundat, and Z. Jacob, Universal spin-momentum locked optical forces, Appl. Phys. Lett. **108**, 061102 (2016).

[25] A. Canaguier-Durand and C. Genet, Transverse spinning of a sphere in a plasmonic field, Phys. Rev. A **89**, 033841 (2014).

[26] A. Aiello, P. Banzer, M. Neugebauer, and G. Leuchs, From transverse angular momentum to photonic wheels, Nat. Photonics **9**, 789 (2015).

[27] Y. N. Nikitin, P. Alonso-González, S. Velez, S. Mastel, A. Centeno, A. Pesquera, A. Zurutuza, F. Casanova, L. E. Hueso, F. H. L. Koppens, and R. Hillenbrand, Real-space mapping of tailored sheet and edge plasmons in graphene nanoresonators, Nat. Photonics **10**, 239 (2016).

[28] Z. Wei, M. D. Goldflam, J.-S. Wu, S. Dai, M. Wagner, A. S. Mcleod, M. K. Liu, K. W. Post, S. Zhu, G. C. A. M. Janssen, M. M. Fogler, and D. N. Basov, Edge and surface plasmons in graphene nanoribbons, Nano Lett. **15**, 8271 (2015).

[29] T. Narushima and H. Okamoto, Strong nanoscale optical activity localized in two-dimensional chiral metal nanostructures, J. Phys. Chem. C **117**, 23964 (2013).

[30] A. F. Oskooi, D. Roundy, M. Ibanescu, P. Bermel, J. D. Joannopoulos, and S. G. Johnson, Meep: A flexible free-software package for electromagnetic simulations by the fdtd method, Comput. Phys. Commun. **181**, 687 (2010).

[31] A. Principi, G. Vignale, M. Carrega, and M. Polini, Intrinsic lifetime of Dirac plasmons in graphene, Phys. Rev. B **88**, 195405 (2013).

[32] W. Wang and J. M. Kinaret, Plasmons in graphene nanoribbons: Interband transitions and nonlocal effects, Phys. Rev. B **87**, 195424 (2013).

[33] S. Thongrattanasiri, A. Manjavacas, and F. J. Garcia de Abajo, Quantum finite-size effects in graphene plasmons, ACS Nano **6**, 1766 (2012).

[34] M. Born, E. Wolf, A. B. Bhatia, P. C. Clemmow, D. Gabor, A. R. Stokes, A. M. Taylor, P. A. Wayman, and W. L. Wilcock, *Principles of Optics: Electromagnetic Theory of Propagation, Interference and Diffraction of Light*, 7th ed. (Cambridge University Press, Cambridge, 1999).

[35] S. J. Orfanidis, *Electromagnetic Waves and Antennas* (Rutgers University, New Brunswick, NJ, 2002).

[36] L. Novotny and B. Hecht, *Principles of Nano-optics* (Cambridge University Press, Cambridge, 2006).